

Transformation of Formazanate at Nickel(II) Centers to Give a Singly Reduced Nickel Complex with Azoimate Radical Ligands and Its Reactivity toward Dioxygen

Deniz Ar, Alexander F. R. Kilpatrick, Beatrice Cula, Christian Herwig, and Christian Limberg*



Cite This: <https://doi.org/10.1021/acs.inorgchem.0c03761>



Read Online

ACCESS |



Metrics & More

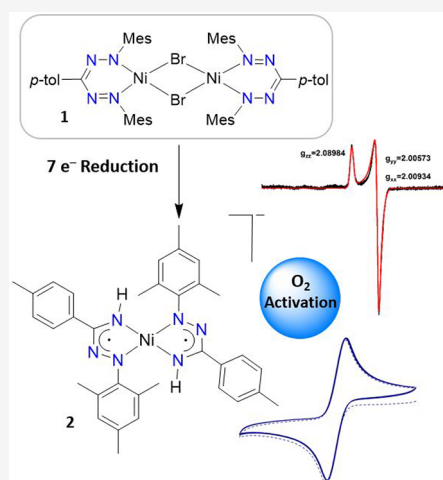


Article Recommendations



Supporting Information

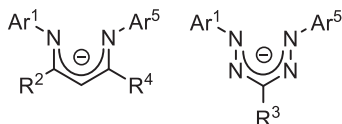
ABSTRACT: The heteroleptic (formazanato)nickel bromide complex $\text{LNi}(\mu\text{-Br})_2\text{NiL}$ [$\text{LH} = \text{Mes-NH-N}=\text{C}(p\text{-tol})\text{-N}=\text{N-Mes}$] has been prepared by deprotonation of LH with NaH followed by reaction with $\text{NiBr}_2(\text{dme})$. Treatment of this complex with KC_8 led to transformation of the formazanate into azoimate ligands via N–N bond cleavage and the simultaneous release of aniline. At the same time, the potentially resulting intermediate complex $\text{L}'_2\text{Ni}$ [$\text{L}' = \text{HN}=\text{C}(p\text{-tol})\text{-N}=\text{N-Mes}$] was reduced by one additional electron, which is delocalized across the π system and the metal center. The resulting reduced complex $[\text{L}'_2\text{Ni}]\text{K}(18\text{-c-6})$ has a $S = 1/2$ ground state and a square-planar structure. It reacts with dioxygen via one-electron oxidation to give the complex $\text{L}'_2\text{Ni}$, and the formation of superoxide was detected spectroscopically. If oxidizable substrates are present during this process, these are oxygenated/oxidized. Triphenylphosphine is converted to phosphine oxide, and hydrogen atoms are abstracted from TEMPO-H and phenols. In the case of cyclohexene, autoxidations are triggered, leading to the typical radical-chain-derived products of cyclohexene.



INTRODUCTION

β -Diketiminatonickel(I) complexes have been shown to reductively activate a wide range of small molecules.^{1–11} A commonly employed synthetic route to β -diketiminatonickel(I) species is treatment of the corresponding nickel(II) halide derivative with KC_8 ^{5,10} or sodium,¹¹ which reduces the metal center, while the β -diketiminato ligand (Chart 1, left) is redox-

Chart 1. (Left) β -Diketiminato Ligand and (Right) Formazanate Ligand



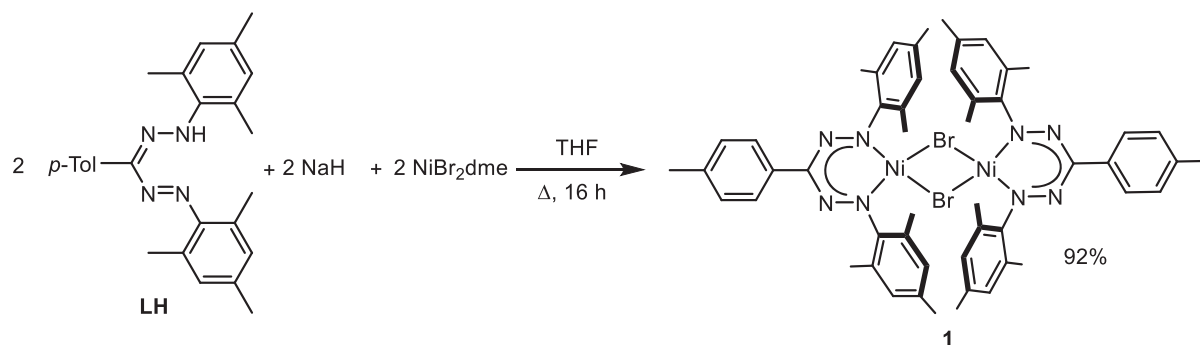
inert. The formazanate ligand (Chart 1, right) is structurally similar but can be reduced to a dianionic (2⁻) form.¹² It therefore, in principle, offers divergent reactivity: the ligand lowest unoccupied molecular orbital (LUMO) is accessible at lower energy,^{13–15} which may allow for reductive activations under milder conditions, and also, in general, ligand-centered redox processes can expand upon the intrinsic reactivity of the metal centers. Hence, exploration of the reduction chemistry of nickel(II) formazanate complexes warranted investigation.

However, suitable precursor compounds for such investigations were not available prior to this work. Homoleptic bis(formazanato)nickel(II) complexes with different substitution patterns at the ligand framework are known,^{16–18} but only one heteroleptic complex has been reported, where two (formazanato)nickel(II) fragments are linked by two bridging hydroxide groups.¹⁷ To perform a reductive dehalogenation, for the reasons outlined above, a (formazanato)nickel(II) halide complex is required. Here we report a representative (formazanato)nickel(II) bromide complex and its reactivity in contact with KC_8 , which leads to reductive cleavage of the formazan N–N bond. This furnishes a nickel(II) complex, which contains two azoimate ligands plus an electron that is delocalized across the entire system and can be removed by dioxygen (O_2) to give superoxide and the corresponding homoleptic nickel(II) complex with two azoimate radical ligands.

Special Issue: Advances in Small-Molecule Activation

Received: December 23, 2020

Scheme 1. Synthesis of Complex 1



RESULTS AND DISCUSSION

For our studies, we chose a formazanate precursor with a tolyl substituent in the R^3 position and mesityl residues for Ar^1 and Ar^5 , i.e., Mes-NH-N=C(*p*-tol)-N=N-Mes (LH).¹² After deprotonation of LH with NaH in tetrahydrofuran (THF) at ambient temperatures and subsequent treatment with NiBr₂(dme), the bromide-bridged dinuclear heteroleptic complex LNi(μ -Br)₂NiL (**1**) was isolated as a green solid in 92% yield (Scheme 1). Elemental analysis and mass spectrometry measurements supported the bulk purity as well as the proposed constitution.

The structure was investigated by X-ray diffraction (XRD) studies performed with suitable single crystals of **1** grown via diffusion of hexane into a THF solution of **1** (Figure 1). In the solid state, 1·3C₄H₈O contains two nickel centers in square-planar coordination spheres. The N–Ni–N angles are 90.34(12)° and 89.60(12)°, whereas the Br–Ni–Br angles are 82.75(18)° and 83.102(18)°, respectively. However, from the side view (Figure 1b), it becomes evident that the nickel formazanate entity as such is not completely planar: The angle between the idealized planes spanned by N8–N5–Ni1–Br1–Br2 and N5–N6–C27–N7–N8 is 19.90(12)°. Likewise, the Ni₂Br₂ core is not planar but bent across the Br⋯Br axis (Figure 1b). The distance between the centers of gravity of the mesityl rings C2–C7 and C44–C49 amounts to 5.2703(4) Å and the one between C18–C23 and C28–C33 to 4.7071(3) Å. This is arguing against π – π stacking between the aryl rings in the solid state.

The ¹H NMR spectrum of **1** dissolved in C₆D₆ (Figure S2) or toluene-*d*₈ shows six sharp signals between δ_H 2 and 8 ppm, consistent with a diamagnetic complex with C_{2v} symmetry on the NMR time scale, as one should expect from the structure determined in the solid state (Figure 1). However, a THF-*d*₈ solution of compound **1** (**1**_{THF}) is NMR-silent, which may indicate a reaction with THF to yield in square-pyramidal nickel coordination, a switch of square planar to tetrahedral coordination, or even the formation of monomers with tetrahedrally coordinated nickel ions. The effective magnetic moment determined by the Evans method^{19,20} was 1.55 μ_B per nickel atom at room temperature, a value consistent with one unpaired electron per metal center. Any paramagnetic nickel(II) ion has two unpaired electrons, and hence the low value for μ_{eff} is suggestive of either a weak magnetic coupling in a dinuclear complex or an equilibrium between complex **1**, with the structure shown in Figure 1, and complex **1**_{THF} with the nickel ions in tetrahedral (or square-pyramidal) coordination spheres. To examine this hypothesis, variable-temperature NMR studies were carried out in 10 K increments between 193

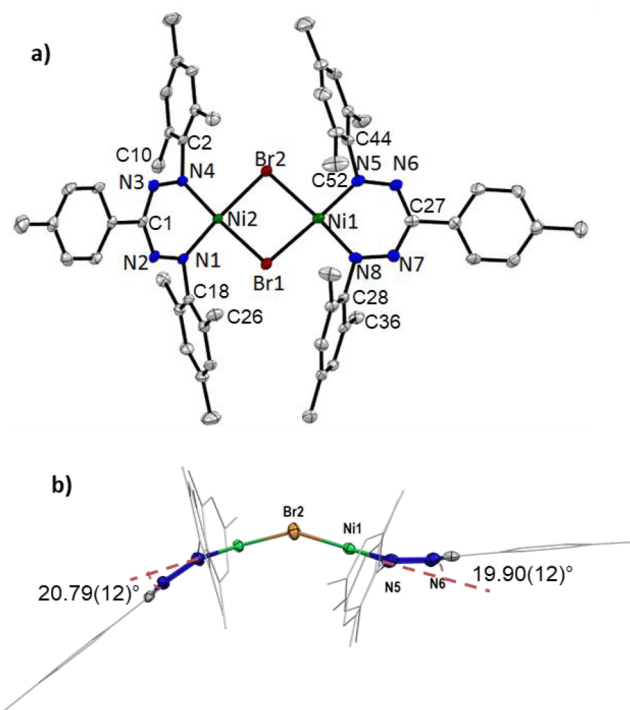
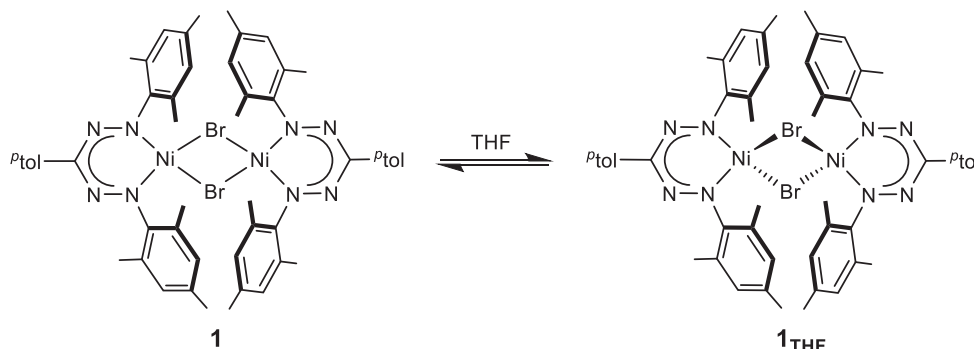


Figure 1. (a) Molecular structure of 1·3THF as determined by single-crystal XRD. Hydrogen atoms and solvent molecules are omitted for clarity. Selected bond lengths [Å] and angles [deg]: Br1–Ni2 2.3557(5), Br1–Ni1 2.3632(6), Br2–Ni2 2.3703(6), Br2–Ni1 2.3793(5), Ni1–N8 1.844(3), Ni1–N5 1.854(3), Ni2–N4 1.841(3), Ni2–N1 1.853(3), N1–N2 1.301(4), N2–C1 1.337(4); Ni2–Br1–Ni1 92.603(19), Ni2–Br2–Ni1 91.832(19), Br1–Ni1–Br2 82.750(18), Br1–Ni2–Br2 83.102(18), N4–Ni2–N1 90.34(12), N8–Ni1–N5 89.60(12), N5–Ni1–Br1 176.31(9), N8–Ni1–Br2 175.35(9). (b) Side view illustrating the nonplanarity of the ligand–nickel entities and Ni₂Br₂ core.

and 298 K. The effective magnetic moment μ_{eff} was found to increase with decreasing temperature to 2.05 μ_B at 193 K, suggesting that the paramagnetic species is favored at low temperatures, which argues against the formation of monomers as the origin of the paramagnetism. At the same time, these observations match the findings already made decades ago for complexes of the type NiL₂X₂ (X = halide), which proved to enter into equilibria involving square-planar (Sp) and tetrahedral (Td) structures.²¹ Solvent-dependent equilibria between the Sp and Td forms are also known. For instance, Mori et al. found out that their homoleptic nickel complexes form equilibria between the Td and Sp conformations in unipolar solvents but have a Td structure in polar solvents.²²

Scheme 2. Proposed Equilibrium between the Square-Planar **1** and Tetrahedral **1**_{THF} in THF

Consequently, we also propose for **1** a solvent- and temperature-dependent equilibrium between Td and Sp molecular structures, as shown in Scheme 2.

With the suitable nickel(II) formazanate precursor compound **1** in hand, its reduction chemistry was studied next, first with the aid of cyclic voltammetry (CV) studies on **1** in a THF solution. These revealed one quasi-reversible redox event at $E_{1/2} = -1.12$ V versus $\text{Fc}^{+/0}$ (Figure 2). For comparison, the

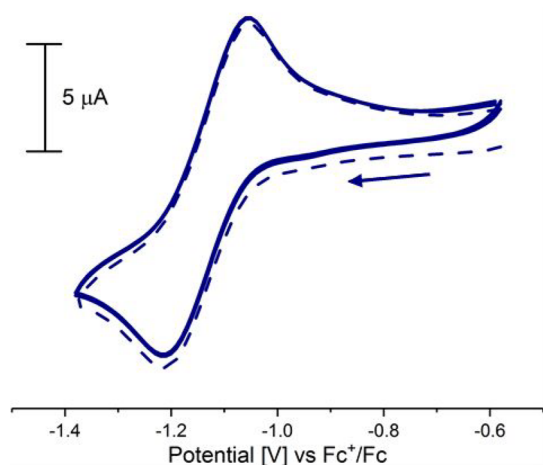


Figure 2. CV curve (two cycles) of **1** dissolved in THF measured at a scan rate of $100 \text{ mV}\cdot\text{s}^{-1}$ (100 mM TBAPF₆ and 1 mM complex **1**) at room temperature. The dotted line denotes the first scan.

homoleptic zinc bis(formazanate) complex L_2Zn reported by Otten and co-workers¹² in 2015 undergoes two ligand-based redox events at -1.80 and -2.30 V. Consequently, it is tempting to assign the redox event at $E_{1/2} = -1.12$ V versus $\text{Fc}^{+/0}$ for **1** to a $\text{Ni}^{\text{II}}/\text{Ni}^{\text{I}}$ redox process [note that a iron(II) bis(formazanate) complex was found to undergo metal-centered reduction at a comparable potential];²³ however, studies on other heteroleptic transition-metal formazanate complexes have clearly shown that the LUMO of formazanate complexes is ligand-centered.^{15,24} Hence, we also assign the process observed for **1** to a reversible ligand-centered reduction. For comparison, the $\text{Ni}^{\text{II}}/\text{Ni}^{\text{I}}$ event of a β -diketiminatonickel(II) bromide complex occurs at -1.37 V (vs Fc/Fc^+).²⁵

On this basis, subsequently the chemical reduction of **1** was investigated. First, complex **1** was reacted with 2 equiv of sodium naphthalenide at -78 °C in toluene for 1 h. The product turned out to be NMR-silent because of paramagnetism. Therefore, an electron paramagnetic resonance

(EPR) spectrum was recorded at 77 K, which showed a signal with corresponding g values of 2.004, 2.008, and 2.013 (Figure S8). This supports the above hypothesis that the reduction is ligand-based. Similar observations were made using $^t\text{BuLi}$ as a mild reductant. Unfortunately, we did not succeed in growing single crystals or isolating a pure product in a different way, so that further investigations were hampered. Investigations on the behavior of **1** toward the stronger reductant KC_8 brought new observations. Upon using 2 equiv of KC_8 a nonuniform reaction was observed to take place, leading to unconsumed starting material and overreduced products, so that we further studied the conversion with excessive amounts of the reagent.

A benzene solution of **1** was stirred for 12 h in the presence of 4 equiv of KC_8 and 4 equiv of 18-crown-6 (18-c-6), which resulted in a color change from green to brown. After filtration over Celite, all volatiles were evaporated and a dark-brown microcrystalline solid was isolated, which was identified by spectroscopic and analytical methods as well as by single-crystal XRD (Figure 3) as $[\text{L}'_2\text{Ni}]\text{K}(18\text{-c-6})$ [**2**; $\text{L}' = \text{HN}=\text{C}(p\text{-tol})\text{-N}=\text{N}\text{-Mes}$] formed with a yield of 45% (Scheme 3).

Crystals suitable for XRD analysis were grown from a concentrated benzene solution, and the solid-state molecular structure (Figure 3) revealed that the formazanate ligands had undergone an N–N cleavage to give ligands with an azoimine backbone.

There is currently no synthetic procedure available for uncoordinated azoimines (Chart 2).²⁶ Coordinated azoimines were reported to form through the reduction of azoiminate ligands,²⁷ and they were also found to be susceptible to reduction with a further electron to give azoiminate radical-anion ligands (Chart 2), the free protonated forms of which are not synthetically accessible, either.^{26,28}

The presence of a $[(18\text{-c-6})\text{K}]^+$ cation in the solid-state structure of **2**· C_6H_6 , as depicted in Figure 3, requires the nickel complex to carry an overall formal charge of 1^- . Considering the square-planar coordination environment of the nickel center, it is reasonable to exclude a nickel(0) oxidation state. This leads to the inference that the associated ligands are anionic in nature, i.e., that they correspond to azoiminate, as shown in Scheme 3, and a third electron then either resides within the ligand system also, so that the nickel atom is in the oxidation state II^+ , or at the nickel center [\rightarrow nickel(I)]. With the background of this hypothesis, the steric and electronic structure of **2** was further analyzed as described below.

Azoiminate are five-electron π systems, and indeed the lengths of the N–N bonds in **2**· C_6H_6 are around 1.383(3) and 1.341(3) Å, respectively, which is typical for delocalized systems containing N–N bonds; also the N–C distances of

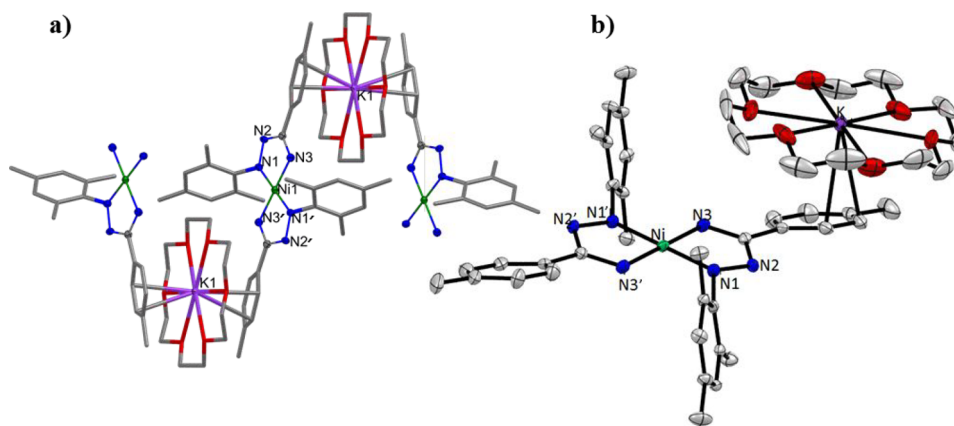


Figure 3. Molecular structure of $2 \cdot C_6H_6$, as determined by single-crystal XRD. Hydrogen and solvent atoms are omitted for clarity. Selected bond lengths [Å] and angles [deg]: Ni–N3 1.832(2), Ni–N1 1.840(2), N1–N2 1.383(3), N2–C1 1.324(3), N3–C1 1.341(3); N3–Ni–N3' 180.0, N3–Ni–N1' 98.43(10), N3–Ni–N1 81.57(10), N2–C1–N3 118.4(2). (a) Polymeric structure of **2**. (b) Single unit of the polymeric structure in part a.

Scheme 3. Reduction of Complex 1 Using KC_8 and 18-c-6, Leading to the Transformation of Formazanate to Azoiminate and the Reduction of the Resulting Complex

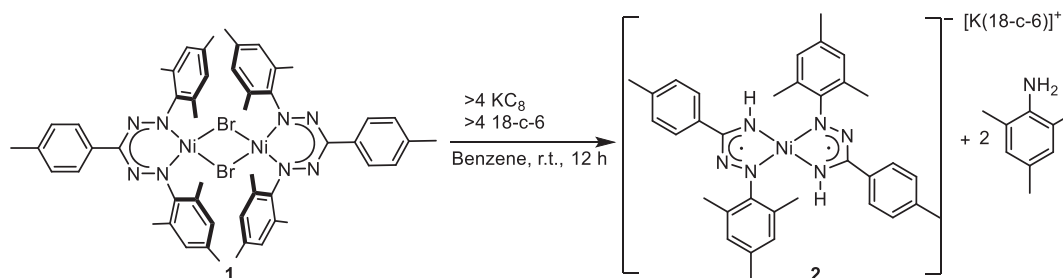


Chart 2. Reduction of Azoimine by One Electron, Leading to the Five-Electron π -System Azoiminate, and by a Second Electron to Yield the Corresponding Diamide



1.324(3) and 1.341(3) Å are consistent with this interpretation.

The counterion $[(18-c-6)K]^+$ interacts via the potassium cation with the *p*-tolyl residues of two neighboring anionic units in a repetitive manner, so that altogether a coordination polymer results with $[(18-c-6)K]^+$ as the linking units. The mesityl substituents are perpendicular to each other, and together with the $[(18-c-6)K]^+$ entities on both sides, they are sterically shielding the nickel center. As mentioned, the coordination sphere of the nickel center is square-planar, which would be untypical for a nickel ion in the oxidation state I+: There are only a few examples of square-planar nickel(I) complexes with neutral ligands in the literature and even fewer with anionic ligands.^{29,30} However, delocalization of the unpaired electron across the ligand π system with maintainance of the oxidation state +II, as revealed by EPR spectroscopy and density functional theory (DFT) calculations (vide infra), explains the structure of **2**.

Two azoiminate ligands contain one unpaired electron each, which are accommodated in the π system, and can be assumed to be strongly coupled antiferromagnetically.^{26,31} Thus, an

additional unpaired electron will likely lead to a $S = 1/2$ ground state, and the question is, where is the unpaired spin density located? To further elucidate the electronic structure of **2**, an EPR spectrum was recorded for a frozen toluene solution at 77 K (Figure 4).

The X-band EPR spectrum of **2** in toluene at 77 K (Figure 4) shows a signal of axial symmetry with the corresponding *g* values of 2.089 and 2.009 consistent with a $S = 1/2$ system. On the one hand, previously reported nickel(I) complexes typically give larger *g* values,^{6,32,33} and, on the other hand, the *g* anisotropy observed in the EPR spectrum of **2** is much larger than that typically observed for hydrocarbon-based radicals. Consequently, the unpaired spin appears to be located both at the ligand and at the metal ion. To support this interpretation, DFT calculations were performed (B3LYP-D3/Def2-TZVP), which indeed confirmed a doublet ground state (quartet 100.6 kJ·mol⁻¹ higher in energy) with only 20% of the unpaired spin density located at the nickel center (Figure 5). Still, in the EPR spectrum, a hyperfine splitting caused by the interaction with nitrogen nuclear spins was not observed, most likely because of the combination of a small coupling constant and the signal

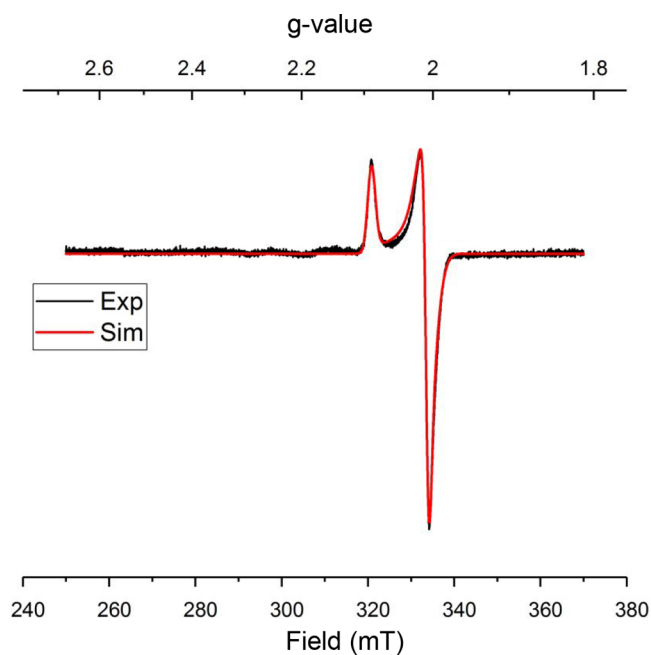


Figure 4. X-band EPR spectrum (77 K, 9.45 GHz) of compound **2** (1 mmol·L⁻¹ in toluene) and simulation (red) for $g_{\parallel} = 2.089$ and $g_{\perp} = 2.009$.

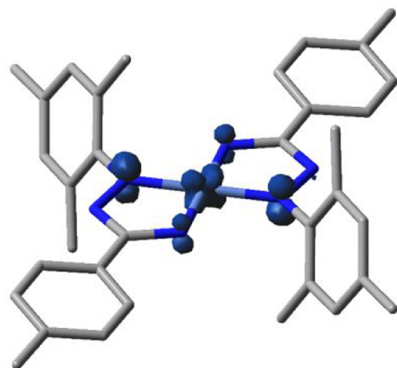


Figure 5. Spin-density distribution calculated for the doublet ground state of complex **2** as an anion without K(18-c-6) (B3LYP-D3/Def2-TZVP).

broadening, which is probably caused by nuclear quadrupole interactions.^{34,35} Wieghardt and co-workers reported a comparable nickel complex, which was generated during spectroelectrochemical studies (EPR coupled with CV) and

for which hyperfine splitting caused by the nitrogen atoms was neither observable.³¹

On the basis of these findings, we conclude that the structure can be viewed best as containing one monoanionic azoiminato ligand as well as one further reduced diamide ligand, as shown in Chart 2 on the right-hand side, with a complete delocalization of both; that is, the extra π electron is shared equally between the two ligands with coupling through a Ni d orbital (on average both ligands are thus in a 1.5-charge state). This fits nicely to the findings made by Wolczanski and co-workers for complexes with nickel in a redox-active ligand framework showing that all redox events were shuttling electrons in and out of the ligand scaffold, thus allowing the nickel center to maintain its favorite oxidation state II+ in a highly stabilizing square-planar coordination sphere.³⁶

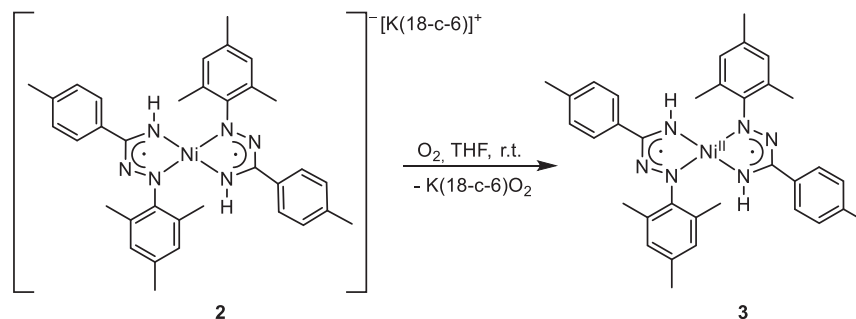
The formation of **2** from **1** in the course of reduction formally leaves behind two “Mes-N:” fragments, which together with four electrons and four protons could form the corresponding aniline, and indeed Mes-NH₂ could be detected after the reaction via ¹H NMR spectroscopy (Figure S4); complex **2** itself is NMR-silent. The conversion of two formazanate ligands into two azoiminato ligands and two aniline equivalents corresponds to a 6e⁻/6H⁺ transformation, which recently has also been observed by Teets and co-workers in attempts to prepare platinum formazanate complexes in ethanol with triethylamine; the latter was assumed to represent the source of the electrons.²⁶ In our case, a further electron reduces the complex, so that altogether seven reduction equivalents are required to realize the reaction in Scheme 3. Consequently, the reaction was repeated with 7 equiv of K⁺C₈ and 18-c-6, and indeed higher yields (70%) of **2** were obtained. The source of the protons in this reaction is still unclear. Analogous reactions using C₆D₆ as the solvent resulted in near-identical product mixtures with no deuterium incorporation, as observed by NMR spectroscopy, and therefore we assume that solvent activation is not responsible.

We then turned our attention to the reactivity of **2**. In particular, its reactivity toward O₂, was of interest to us, given the precedence for isolable nickel(II) superoxide complexes after O₂ activation.³⁷

The reaction of **2** with 1 atm of O₂ was carried out in THF or toluene at ambient temperatures (Scheme 4), resulting in a color change from brown to green. After workup, L₂Ni (**3**) was isolated, derived from **2** by a single-electron oxidation, as already indicated by the absence of a cation.

Single crystals of **3** were grown by diffusion of pentane into a benzene solution of **3** stored at room temperature. The molecular structure (Figure S19) reveals a nickel center

Scheme 4. Oxidation of Complex **2** by O₂ in THF at Ambient Temperatures



surrounded by four nitrogen atoms in a square-planar fashion; that is, the core of **2** has been retained, but there are some differences in the bond lengths. The Ni–N bonds are shorter in **3** than in **2**, for instance, the Ni–N2 distance by 0.027 Å. Most significantly, the N–N distances are, on average, 0.046 Å shorter in **3** than in **2**. Furthermore, the N2–C1 bond is elongated, whereas N3–C1 is shortened, which is reasonable because participation of the diamide ligand (through the extra electron) is not relevant anymore.

The removal of an electron from **2** leaves two azoimino radical ligands in **3**, and as judged by the diamagnetism of **3** (according to ^1H NMR and EPR spectroscopy), their unpaired electrons are coupled strongly antiferromagnetically, as expected (*vide supra*). Indeed, DFT calculations also suggested an open-shell singlet ground state with unpaired spin density mainly located at the nitrogen atoms binding the mesityl residues (Figure S21). The CV studies of **3** in THF revealed a redox event at $E_{1/2} = -1.45$ V versus $\text{Fc}^{+/0}$ (Figure 6), which is fully reversible, as expected, considering the stability of both **2** and **3**, for which only minimal structural change occurs upon electron transfer.

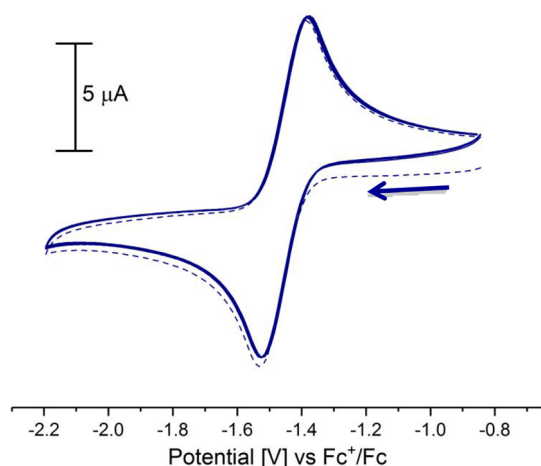


Figure 6. Overlaid CV scans of **3** measured at a scan rate of 100 $\text{mV}\cdot\text{s}^{-1}$ in THF (100 mM TBAPF₆ and 0.05 $\text{mmol}\cdot\text{L}^{-1}$ complex **3**) at room temperature. The dotted line denotes the first scan.

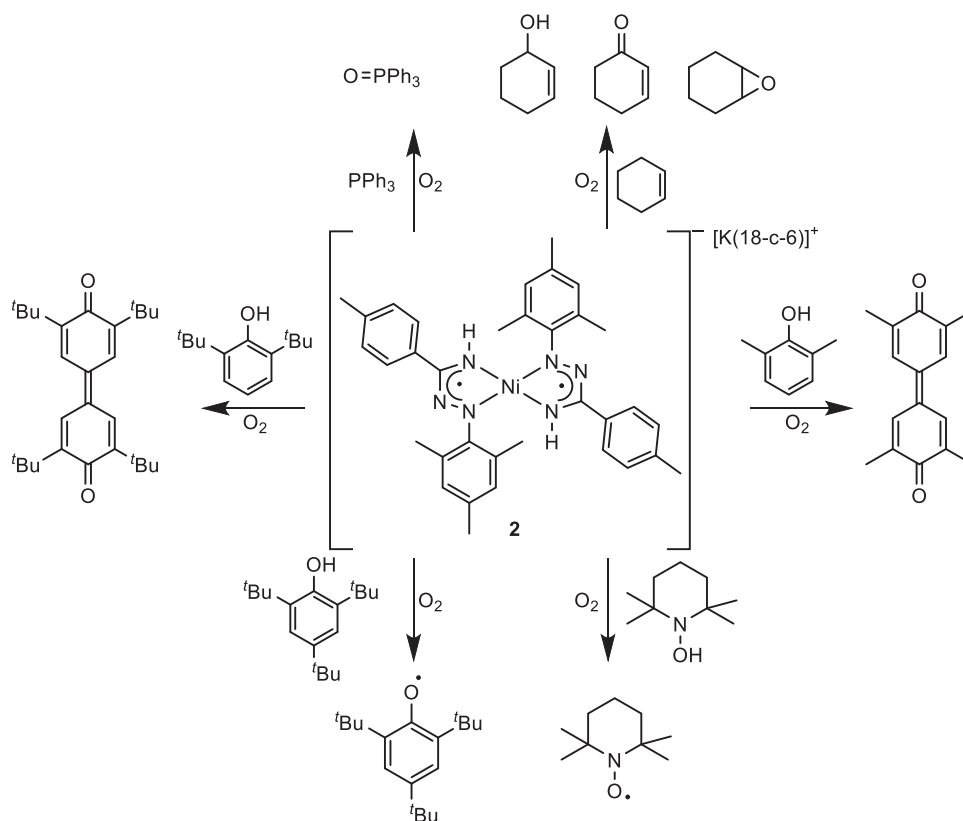
In the reaction between **2** and O_2 , electron transfer will lead initially to a superoxide and thus potentially to a nickel(II) superoxide intermediate (if the contact occurs via the metal).³⁸ In order to gather any information on such an intermediate, the reaction between **2** and O_2 was monitored by variable-temperature UV–vis spectroscopy between -80 °C and room temperature in THF and toluene (Figure S14). In all UV–vis experiments, a new band belonging to the final product **3** arose around 720 nm, immediately after the addition of O_2 . This low-energy band is best assigned to the HOMO-to-LUMO transition, which has a ligand-to-metal charge-transfer character and is responsible for the strong luscious green color of the complex. Teets and co-workers reported UV–vis studies on various platinum azoimino complexes, which also showed bands at ca. 720 nm.²⁶ However, the UV–vis experiments did not reveal bands evolving/decaying before those of the final product **3**; i.e., there was no evidence for an intermediate with a sufficiently long lifetime. Cryo-stopped-flow experiments performed at -40 °C in THF did not allow for the detection of any transient species. Consequently, the

oxidation of **2** by O_2 is either an outer-sphere process or the formed encounter complex rather quickly dissociates to give **3** and potassium superoxide.

Notably, free superoxide (likely in interaction with a K^+ cation) could be detected by EPR. An EPR spectrum recorded after the reaction between compound **2** and O_2 showed a signal with a small g anisotropy and a g tensor of 2.045, 2.009, and 2.004, i.e., close to the value of the free electron (Figure S9). These g values are very similar to those reported by Fukuzumi and Ohkubo found for superoxide anions stabilized by a variety of different metal ions.³⁹ These researchers postulated that the interaction with a potassium ion should increase g_{zz} compared to the values observed for lithium (LiO_2 : $g_{zz} = 2.0546$) and sodium (NaO_2 : $g_{zz} = 2.0841$) cations. As mentioned above, after the reaction between **2** and O_2 , the observed signal had a g_{zz} value of 2.045, that is, lower than one should expect, which may be a consequence of the additional presence of 18-c-6 and a solvent. Indeed, in 2011, Büchner and co-workers found that 18-c-6 leads to a line broadening of the EPR spectrum of the superoxide radical anion and also changes of the g anisotropy.⁴⁰

Apparently, binding of the superoxide radical anion to the nickel center is not favorable, likely because of the relatively stable square-planar coordination environment of the nickel(II) center in **3**. However, this is the basis on which many catalysts employed industrially for oxidation reactions with O_2 work.⁴¹ In the first step, a metal compound transfers an electron to produce a superoxide, which reacts with the organic substrate, and then radical-chain processes are initiated (autoxidations); the main function of the metal catalyst is the initiation of the reaction and in some systems also the splitting of the hydroperoxide intermediates.⁴¹ Such “homolytic oxidation reactions” naturally have the disadvantage that the selectivity is low and (because radicals determine the proceedings) they are difficult to control, so that “heterolytic oxidation reactions”, which proceed via well-defined active oxygen–metal complexes, are clearly favorable. However, there are only a few examples of the latter, which successfully work *catalytically* with O_2 ,⁴² and, on the other hand, there are cases where even homolytic oxidations can be performed with high selectivity.⁴¹

To investigate the potential of **2**/ O_2 to perform oxidative conversions, the reactions of several organic substrates with **2**/ O_2 were monitored using different analytical methods after confirmation that the substrates alone do not react with **2** or O_2 under the same conditions (Scheme 5) and different methods were used to detect the oxidation products (Table 1). To examine whether **2** can trigger and promote autoxidation, it was tested in the solvent-free system cyclohexene/ O_2 . Compound **2** was suspended in cyclohexene, and O_2 was bubbled into the solution for 30 s, followed by stirring for 16 h at ambient temperatures. Upon the addition of O_2 , the color of the solution changes to green. Indeed, the oxidation products 1,2-epoxycyclohexane, 2-cyclohexen-1-one, and 2-cyclohexen-1-ol could be identified in a ratio of 1:8:7.5, employing gas chromatography coupled to mass spectrometry (GC/MS; TON = 8; Figure S13). On the basis of the nature of these products, this reaction follows a radical-chain reaction mechanism proposed by Wei et al.⁴³ in 2016 and Kohantorabi et al.⁴⁴ in 2018. In the first step, a cyclohexenyl radical is produced that can be converted to a peroxy radical. This can abstract a hydrogen atom to form ROOH (R = cyclohexenyl) or react further to produce 2-cyclohexen-1-one and cyclo-

Scheme 5. Reactivity of Complex 2 toward O₂ in the Presence of Various SubstratesTable 1. Reaction Products Formed in the Oxidation of Different Substrates with the Combination of Complex 2 and O₂ and Their Characterization

substrate	reaction conditions	product(s)	identification
triphenylphosphine	C ₆ D ₆ at rt	triphenylphosphine oxide	³¹ P NMR = 24 ppm
cyclohexene	neat at rt	1,2-epoxycyclohexane, 2-cyclohexen-1-one, and 2-cyclohexen-1-ol	GC/MS
2,6-dimethylphenol	toluene, -40 °C to rt	3,3',5,5'-tetramethyl-4,4-diphenylquinone	UV-vis
2,6-di-tert-butylphenol	toluene, -80 °C to rt	3,3',5,5'-tetra-tert-butyl-4,4-diphenylquinone	UV-vis
TEMPO-H	toluene, rt	TEMPO	EPR at 77 K
2,4,6-tri-tert-butylphenol	THF, rt	TTBP radical	EPR at 77 K

hexen-1-ol; ROOH is also decomposing to these products. Hence, complex 2 can activate molecular oxygen for the autoxidation of substrates under mild conditions.

Complex 2 also mediates oxygen-atom transfer from O₂, as demonstrated by the reaction with triphenylphosphine. ³¹P NMR spectroscopy in C₆D₆ revealed that 2 equiv of PPh₃ were oxidized by O₂ in the presence of 1 equiv of complex 2 to give triphenylphosphine oxide (Figure S1). The evolution of the signal for OPPh₃ started immediately after the addition of O₂, and the reaction reached completion within 15 h. Interestingly, the EPR signal assigned to superoxide was not observed for mixtures of 2 and O₂ in the presence of PPh₃. After 15 h, the reaction mixture was completely EPR-silent (Figure S12).

Furthermore, TEMPO-H and phenols [2,4,6-tri-tert-butylphenol (TTBP), 2,6-dimethylphenol (DMP), and 2,6-di-tert-butylphenol (DTBP)] were employed to test the potential of 2/O₂ to perform hydrogen-atom abstraction. Therefore, complex 2 (0.5 mmol·L⁻¹), in combination with O₂, was reacted with TEMPO-H (25 mmol·L⁻¹ in toluene) and TTBP (12.5 mmol·L⁻¹ in THF), respectively, at room temperature for 30 min. The reaction mixtures were then analyzed by EPR spectroscopy at 77 K, which revealed the corresponding signals typical for the radicals formed upon hydrogen-atom abstraction from these substrates (conversion of ~1 equiv; Figures S10 and S11).^{45–47} The reactions with DMP and DTBP were investigated using toluene as well as THF as solvents at different temperatures by UV-vis spectroscopy. In both cases, a new band at 425 nm was observed, indicating formation of the coupling products 3,3',5,5'-tetra-tert-butyl-4,4-diphenylquinone and 3,3',5,5'-tetramethyl-4,4-diphenylquinone, confirming that 2/O₂ is capable of abstracting a hydrogen atom from DMP and DTBP also (Figures S15–S17).

CONCLUSION

We have synthesized the first heteroleptic (formazanato)-nickel(II) bromide complex and examined its redox behavior. In attempts to reduce this complex with KC₈ in the presence of 18-c-6, formazanate did not remain intact but underwent N–N bond cleavage, which seems to be a potential decomposition reaction of formazanate complexes in reduced states. As a consequence, the formazanate ligands transformed into azoiminato ligands, which contain an unpaired electron in the π system and cannot be prepared, currently, in free (protonated) form by any synthetic procedure. The resulting

complex was further reduced by one electron, yielding **2**, where the extra electron is delocalized across the entire complex plane so that formally the two ligands are in an average 1.5–charge and a $S = 1/2$ ground state results. In contact with O_2 , this electron is removed, leading to free superoxide and **3**, in which the two azoiminato radical ligands are coupled antiferromagnetically, so that the complex is diamagnetic. O_2 activation at **2** can be utilized to oxidize organic and inorganic substrates. In the presence of cyclohexene, autoxidation is triggered, leading to the typical radical-chain-derived oxidation products. Triphenylphosphine is converted into the corresponding oxide, and hydrogen atoms are abstracted from TEMPO-H and phenols.

EXPERIMENTAL SECTION

General Considerations. All manipulations were carried out in a glovebox or by using Schlenck-type techniques under a dry argon atmosphere. Microanalyses were performed with a Leco CHNS-932 elemental analyzer. UV–vis spectra were recorded at variable temperatures using an Agilent 8453 UV–vis spectrophotometer equipped with a quartz dewar. Cryo-stopped-flow experiments were performed by using a SFM-2000/s stopped flow mixer from Bio-Logic Science Instruments, a high-power UV–vis fiber light source from Hamamatsu, and a Tidas MMS vis/NIR from J&M Analytik AG. The temperature was controlled by a cryostat from Huber with isopropyl alcohol as a cooling agent. Attenuated-total-reflectance infrared (ATR-IR) spectra were recorded with a Bruker Alpha Fourier transform infrared spectrometer. EPR spectra were measured on an ESR Miniscope MS5000 (Magnetech), equipped with a quartz finger dewar. All spectra were quantified against a copper(II) standard, and to determine the g values, spectra were simulated with *Easyspin*. Electrospray ionization mass spectrometry (ESI/MS) spectra were carried out on an Agilent Technologies 6210 time-of-flight liquid chromatography–mass spectrometry instrument. GC analysis was carried out by using an Agilent 7890B gas chromatograph (HP5 column, 30 m) with a flame-ionization detector coupled to an Agilent 5977B electron impact mass spectrometry (EI-MS) spectrometer with a triple-axis detector. The instrument was equipped with an Agilent G4513A autoinjector (injection of approximately 10 μ L). Specifications for Method 5: The GC method starts with an oven temperature of 50 $^{\circ}$ C (hold time 5 min) and includes two ramps (ramp 1, 50–190 $^{\circ}$ C, 10 $^{\circ}$ C \cdot min $^{-1}$; ramp 2, 190–300 $^{\circ}$ C, 20 $^{\circ}$ C \cdot min $^{-1}$), a total run time of 24.5 min, and a solvent delay of 2.9 min. MS peaks were analyzed and compared with the library database of NIST MS Search 2.3. All EI-MS spectra of the detected peaks were in good agreement with the library database of the expected substances. NMR spectra were measured using a Bruker 300 MHz DPX instrument (1 H NMR 300 MHz). Electrochemical studies were carried out using a PalmSens EmStat Blue potentiostat under computer control. CV experiments were performed under an argon atmosphere using a three-electrode configuration with a glassy carbon disk (7.0 mm 2) as the working electrode for complex **3** and gold as the working electrode for complex **1**, a platinum wire as the counter electrode, and a silver wire as the pseudoreference electrode. Sample solutions were prepared by dissolving the analyte (ca. 5 mmol \cdot L $^{-1}$) in THF (3.0 cm 3), followed by the addition of a supporting electrolyte, [n Bu $_4$ N][PF $_6$]. The reported midpeak potentials are referenced internally to that of the FeCp $_2^{+/0}$ redox couple, which was measured by adding ferrocene (ca. 0.5 mg) to the sample solution. Crystallographic data collection was performed with a Bruker D8 Venture diffractometer at 100 K, using Mo $K\alpha$ radiation ($\lambda = 0.71073$ Å). The data collections were performed with a Bruker D8 VENTURE area detector with Mo $K\alpha$ radiation ($\lambda = 0.71073$ Å). Multiscan absorption corrections, implemented in SADABS,⁴⁸ were applied to the data. The structures were solved by an intrinsic phasing method⁴⁹ and refined by full-matrix least-squares procedures based on F^2 with all measured reflections⁵⁰ with anisotropic temperature factors for all non-hydrogen

atoms. All hydrogen atoms were added geometrically and refined by using a riding model.

Chemicals. 1,5-Dimesityl-3-(*p*-tolyl)formazan, NiBr $_2$ dme, and KC $_8$ were synthesized according to literature procedures.^{12,51,52} NaH was purchased from Sigma-Aldrich and used as received. TEMPO-H was produced according to a modified literature procedure.^{53,54} O_2 was added via a balloon for the UV–vis experiments. For all other O_2 -involving experiments, the atmosphere in the reaction vessel was exchanged by an O_2 atmosphere.

Solvents. All solvents were degassed prior to use. Toluene, *n*-hexane, pentane, and dichloromethane (DCM) were purified by employing an MBraun Solvent Purification System SPS, stored over a potassium mirror in Young Schlenk tubes. Pentane and DCM were stored over molecular sieves (3 Å). Benzene was purchased from Sigma-Aldrich and stored over a potassium mirror. THF was purchased from Acros Organics, distilled over sodium, and stored over molecular sieves (3 Å).

(L'NiBr) $_2$ (**1**). A total of 100 mg of 1,5-dimesityl-3-(*p*-tolyl)formazan (1 equiv, 0.25 mmol) was dissolved in 12 mL of THF, and NaH (6.6 mg, 1.1 equiv, 0.27 mmol) was added. After stirring overnight at room temperature, the reaction mixture was added to a suspension of NiBr $_2$ (dme) (85.2 mg, 1.10 equiv, 0.27 mmol) in 10 mL of THF. After refluxing at 80 $^{\circ}$ C for 16 h, the resulting green solution was filtered, and all volatiles were removed under reduced pressure. The green solid was extracted with benzene and freeze-dried under reduced pressure (144 mg, 0.13 mmol, 92%). Elem anal. Found for C $_{52}$ H $_{58}$ Br $_2$ N $_8$ Ni $_2$ (1072.72 g \cdot mol $^{-1}$): H, 5.80; C, 58.28; N, 10.13. Calcd: H, 5.45; C, 58.25; N, 10.45. 1 H NMR (300.1 MHz, C $_6$ D $_6$): δ 7.89 (d, 2H, $J = 8.45$ Hz), 6.97 (d, 2H, $J = 8.45$ Hz), 6.50 (s, 4H), 2.46 (s, 12H), 2.10 (s, 6H), 2.03 (s, 3H). 13 C{ 1 H} NMR (75.47 MHz, C $_6$ D $_6$): δ 149.8, 137.1, 135.8, 131.3, 129.2, 124.4, 20.7, 19.0. ESI/MS (MeCN, positive-ion mode): m/z 504.162 (LNiCNNa $^+$). Calcd: m/z 504.17. IR (ATR-IR; cm $^{-1}$): $\tilde{\nu}$ 2967, 2946, 2916, 2855, 1652, 1605, 1515, 1473, 1434, 1374, 1329, 1306, 1279, 1187, 1137, 1070, 1038, 990, 952, 876, 822, 765, 660, 627, 574, 530, 517, 463, 430.

[L' $_2$ Ni][K(18-c-6)] (**2**). **1** (1 equiv, 80 mg, 74.16 μ mol) was dissolved in benzene. KC $_8$ (7.5 equiv, 75.7 mg, 556.2 μ mol) and 18-c-6 (7.5 equiv, 147 mg, 556.2 μ mol) were added to the solution. After stirring for 12 h at room temperature, the dark-brown reaction mixture was filtered over Celite, and all volatiles were removed under reduced pressure. The resulting brown solid was washed with *n*-hexane and dried overnight in vacuo to yield **2**. However, **2** thus obtained was often contaminated somewhat by (18-c-6)KBr, which has rather similar properties and also crystallizes together with **2**. On average, the yield of **2**, determined by weighing the product and subtracting the portion of (18-c-6)KBr according to elemental analysis, was 70%. Crystals of **2** suitable for XRD were grown from a concentrated benzene solution at room temperature. Elem anal. Found for a pure sample of **2** (C $_{52}$ H $_{68}$ KN $_6$ NiO $_6$; 892.83 g \cdot mol $^{-1}$): H, 6.99; C, 62.38; N, 8.85. Calcd: H, 7.00; C, 61.88; N, 9.41. ATR-IR (crystal; cm $^{-1}$): $\tilde{\nu}$ 2888, 1598, 1554, 1510, 1492, 1467, 1425, 1399, 1391, 1369, 1351, 1290, 1252, 1212, 1204, 1173, 1156, 1100, 1047, 1008, 960, 836, 821, 779, 741, 732, 714, 683, 657, 640, 621, 581, 522, 501, 475, 465, 428.

L' $_2$ Ni (**3**). **2** (20 mg, 22.72 μ mol) was dissolved in 2 mL of THF, and O_2 was bubbled into the solution. After 1 h of stirring at ambient temperature, the reaction mixture was filtered, and all of the volatiles were removed under reduced pressure. After washing of the residue with *n*-hexane and toluene, 14.5 mg of a green solid was obtained. This consisted mainly of **2** but also contained some (18-c-6)KBr that had been introduced into the system as an impurity of **2** and yet again was difficult to separate. Elem anal. Found for C $_{34}$ H $_{38}$ N $_6$ Ni $^{1/2}$ C $_{12}$ H $_{24}$ O $_6$ KBr (781.07 g \cdot mol $^{-1}$): H, 6.43; C, 61.13; N, 10.32. Calcd: H, 6.45; C, 61.51; N, 10.76. Because elemental analysis indicated a ratio of **3** to (18-c-6)KBr of 1:0.5, the yield of **3** can be determined to 11.5 mg (19.50 μ mol, 85%). 1 H NMR (300.1 MHz, CD $_2$ Cl $_2$): δ 7.48 (d, 2H, $J = 8.28$ Hz), 7.16 (d, 2H, $J = 8.28$ Hz), 7.06 (s, 2H), 6.45 (s, NH), 2.43 (s, 3H), 2.37 (s, 6H), 2.34 (s, 3H). 13 C{ 1 H} NMR (75.47 MHz, CD $_2$ Cl $_2$): δ 18.9, 21.3, 26.0, 126.3, 128.7, 129.7, 133.8, 137.0, 140.0. ESI/MS (MeCN, positive-ion

mode): m/z 589.41 (L'_2NiH^+). Calcd: m/z 589.25. ATR-IR (crystal; cm^{-1}): $\tilde{\nu}$ 2889, 1718, 1652, 1603, 1524, 1472, 1454, 1417, 1351, 1300, 1282, 1259, 1226, 1165, 1102, 1017, 961, 835, 797, 704.

■ ASSOCIATED CONTENT

SI Supporting Information

The Supporting Information is available free of charge at <https://pubs.acs.org/doi/10.1021/acs.inorgchem.0c03761>.

NMR, EPR and GC measurements, UV-vis studies, crystal data, and DFT calculations (PDF)

Accession Codes

CCDC 2049782–2049784 contain the supplementary crystallographic data for this paper. These data can be obtained free of charge via www.ccdc.cam.ac.uk/data_request/cif, or by emailing data_request@ccdc.cam.ac.uk, or by contacting The Cambridge Crystallographic Data Centre, 12 Union Road, Cambridge CB2 1EZ, UK; fax: +44 1223 336033.

■ AUTHOR INFORMATION

Corresponding Author

Christian Limberg – *Institut für Chemie, Humboldt-Universität zu Berlin, 12489 Berlin, Germany*; orcid.org/0000-0002-0751-1386; Phone: +4930-20937382; Email: Christian.limberg@chemie.hu-berlin.de

Authors

Deniz Ar – *Institut für Chemie, Humboldt-Universität zu Berlin, 12489 Berlin, Germany*

Alexander F. R. Kilpatrick – *Institut für Chemie, Humboldt-Universität zu Berlin, 12489 Berlin, Germany*; orcid.org/0000-0002-2108-2709

Beatrice Cula – *Institut für Chemie, Humboldt-Universität zu Berlin, 12489 Berlin, Germany*; orcid.org/0000-0001-6262-4925

Christian Herwig – *Institut für Chemie, Humboldt-Universität zu Berlin, 12489 Berlin, Germany*

Complete contact information is available at:

<https://pubs.acs.org/doi/10.1021/acs.inorgchem.0c03761>

Notes

The authors declare no competing financial interest.

■ ACKNOWLEDGMENTS

We are grateful to the Humboldt-Universität zu Berlin for financial support and the Deutsche Forschungsgemeinschaft (German Research Foundation) for funding under Germany's Excellence Strategy EXC 2008/1-390540038s. We also thank the groups of Prof. Dr. Klaus Lips and Dr. Boris Naydenov from Helmholtz Zentrum Berlin for providing us with access to EPR instruments.

■ REFERENCES

- (1) Puiui, S. C.; Warren, T. H. Three-Coordinate β -Diketiminato Nickel Nitrosyl Complexes from Nickel(I)–Lutidine and Nickel(II)–Alkyl Precursors. *Organometallics* **2003**, *22*, 3974–3976.
- (2) Eckert, N. A.; Dinescu, A.; Cundari, T. R.; Holland, P. L. A T-shaped three-coordinate nickel (I) carbonyl complex and the geometric preferences of three-coordinate d^9 complexes. *Inorg. Chem.* **2005**, *44*, 7702–7704.
- (3) Kogut, E.; Wiencko, H. L.; Zhang, L.; Cordeau, D. E.; Warren, T. H. A Terminal Ni(III)–Imide with Diverse Reactivity Pathways. *J. Am. Chem. Soc.* **2005**, *127*, 11248–11249.

- (4) Yao, S.; Bill, E.; Milsmann, C.; Wieghardt, K.; Driess, M. A “Side-on” Superoxonickel Complex [LNi(O₂)] with a Square-Planar Tetracoordinate Nickel(II) Center and its Conversion into [LNi(μ -OH)₂Ni]. *Angew. Chem., Int. Ed.* **2008**, *47*, 7110–7113.

- (5) Pfirrmann, S.; Limberg, C.; Herwig, C.; Stöber, R.; Ziemer, B. A Dinuclear Nickel(I) Dinitrogen Complex and its Reduction in Single-Electron Steps. *Angew. Chem., Int. Ed.* **2009**, *48*, 3357–3361.

- (6) Horn, B.; Limberg, C.; Herwig, C.; Braun, B. Nickel(I)-mediated transformations of carbon dioxide in closed synthetic cycles: reductive cleavage and coupling of CO₂ generating Ni(I)CO, Ni(II)CO₃ and Ni(II)C₂O₄ Ni(II) entities. *Chem. Commun.* **2013**, *49*, 10923–10925.

- (7) Holze, P.; Horn, B.; Limberg, C.; Matlachowski, C.; Mebs, S. The Activation of Sulfur Hexafluoride at Highly Reduced Low-Coordinate Nickel Dinitrogen Complexes. *Angew. Chem., Int. Ed.* **2014**, *53*, 2750–2753.

- (8) Duan, P.-C.; Manz, D.-H.; Dechert, S.; Demeshko, S.; Meyer, F. Reductive O₂ Binding at a Dihydride Complex Leading to Redox Interconvertible μ -1,2-Peroxo and μ -1,2-Superoxo Dinickel(II) Intermediates. *J. Am. Chem. Soc.* **2018**, *140*, 4929–4939.

- (9) Kothe, T.; Kim, U. H.; Dechert, S.; Meyer, F. Reductive Binding of Nitro Substrates at a Masked Dinickel(I) Complex and Proton-Coupled Conversion to Reduced Nitroso Ligands. *Inorg. Chem.* **2020**, *59*, 14207–14217.

- (10) Holze, P.; Braun-Cula, B.; Mebs, S.; Limberg, C. Stabilization of β -Diketiminato Nickel(I) with Alkaline Metal Halide Entities for Small Molecule Activation. *Z. Anorg. Allg. Chem.* **2018**, *644*, 973.

- (11) Horn, B.; Pfirrmann, S.; Limberg, C.; Herwig, C.; Braun, B.; Mebs, S.; Metzinger, R. N₂ Activation in Ni^I-NN-Ni^I units: The Influence of Alkali Metal Cations and CO Reactivity. *Z. Anorg. Allg. Chem.* **2011**, *637*, 1169.

- (12) Chang, M.-C.; Roewen, P.; Travieso-Puente, R.; Lutz, M.; Otten, E. Formazanate ligands as structurally versatile, redox-active analogues of β -diketiminates in zinc chemistry. *Inorg. Chem.* **2015**, *54*, 379–388.

- (13) Milocco, F.; Demeshko, S.; Meyer, F.; Otten, E. Ferrate(II) complexes with redox-active formazanate ligands. *Dalton Trans.* **2018**, *47*, 8817–8823.

- (14) Gilroy, J. B.; Otten, E. Formazanate coordination compounds: synthesis, reactivity, and applications. *Chem. Soc. Rev.* **2020**, *49*, 85–113.

- (15) Broere, D. L.; Mercado, B. Q.; Lukens, J. T.; Vilbert, A. C.; Banerjee, G.; Lant, H. M.; Lee, S. H.; Bill, E.; Sproules, S.; Lancaster, K. M.; Holland, P. L. Reversible Ligand-Centered Reduction in Low-Coordinate Iron Formazanate Complexes. *Chem. - Eur. J.* **2018**, *24*, 9417–9425.

- (16) Tezcan, H.; Uzluk, E.; Aksu, M. L. Synthesis, spectroscopic and electrochemical studies on bis-[1,3-substituted (Cl, Br) phenyl-5-phenyl formazanato]nickel(II) complexes. *Spectrochim. Acta, Part A* **2008**, *70*, 973–982.

- (17) Gilroy, J. B.; Patrick, B. O.; McDonald, R.; Hicks, R. G. Transition metal complexes of 3-cyano- and 3-nitroformazans. *Inorg. Chem.* **2008**, *47*, 1287–1294.

- (18) Frolova, N. A.; Vatsadze, S. Z.; Zavodnik, V. E.; Rakhimov, R. D.; Zyk, N. V. Pyridine-containing nickel(II) bis-formazanates: Synthesis, structure, and electrochemical study. *Russ. Chem. Bull.* **2006**, *55*, 1810–1818.

- (19) Evans, D. The determination of the paramagnetic susceptibility of substances in solution by nuclear magnetic resonance. *J. Chem. Soc.* **1959**, 2003–2005.

- (20) Schubert, E. M. Utilizing the Evans method with a superconducting NMR spectrometer in the undergraduate laboratory. *J. Chem. Educ.* **1992**, *69*, 62.

- (21) Cotton, F. A. *Advanced Inorganic Chemistry, A Comprehensive Text*, 4th ed.; Wiley: New York, 1980.

- (22) Mori, Y.; Shirase, H.; Fukuda, Y. Substituent and Solvent Effects on Square-Planar–Tetrahedral Equilibria of Bis[4-(arylimino)pentan-2-onato]nickel(II) and Bis[1-aryl-3-(phenylimino)butan-1-onato]nickel(II) Complexes. *Bull. Chem. Soc. Jpn.* **2008**, *81*, 1108–1115.

- (23) Travieso-Puente, R.; Broekman, J. O. P.; Chang, M.-C.; Demeshko, S.; Meyer, F.; Otten, E. Spin-Crossover in a Pseudo-tetrahedral Bis(formazanate) Iron Complex. *J. Am. Chem. Soc.* **2016**, *138*, 5503–5506.
- (24) Kabir, E.; Wu, C.-H.; Wu, J. I. C.; Teets, T. S. Heteroleptic Complexes of Cyclometalated Platinum with Triarylformazanate Ligands. *Inorg. Chem.* **2016**, *55*, 956–963.
- (25) Zimmermann, P.; Kilpatrick, A. F. R.; Ar, D.; Demeshko, S.; Cula, B.; Limberg, C. Electron transfer within β -diketiminato nickel bromide and cobaltocene redox couples activating CO₂. *Chem. Commun.* **2021**, *57*, 875–878.
- (26) Mu, G.; Cong, L.; Wen, Z.; Wu, J. I. C.; Kadish, K. M.; Teets, T. S. Homoleptic Platinum Azo-iminate Complexes via Hydrogenative Cleavage of Formazans. *Inorg. Chem.* **2018**, *57*, 9468–9477.
- (27) Pramanik, S.; Roy, S.; Ghorui, T.; Ganguly, S.; Pramanik, K. Iridium(III) Mediated Reductive Transformation of Closed-Shell Azo-Oxime to Open-Shell Azo-Imine Radical Anion: Molecular and Electronic Structure, Electron Transfer, and Optoelectronic Properties. *Inorg. Chem.* **2016**, *55*, 1461–1468.
- (28) Pal, C. K.; Chattopadhyay, S.; Sinha, C.; Chakravorty, A. A Bis(azo-imine)palladium(II) System with 10 Ligand π Electrons. Synthesis, Structure, Serial Redox, and Relationship to Bis-(azooximates) and Other Species. *Inorg. Chem.* **1996**, *35*, 2442–2447.
- (29) Banerjee, S.; Sheet, D.; Sarkar, S.; Halder, P.; Paine, T. K. Nickel complexes of ligands derived from (*o*-hydroxyphenyl) dichalcogenide: delocalised redox states of nickel and *o*-chalcogenophenolate ligands. *Dalton Trans.* **2019**, *48*, 17355–17363.
- (30) Lin, C.-Y.; Power, P. P. Complexes of Ni(i): a “rare” oxidation state of growing importance. *Chem. Soc. Rev.* **2017**, *46*, 5347–5399.
- (31) Blanchard, S.; Neese, F.; Bothe, E.; Bill, E.; Weyhermüller, T.; Wieghardt, K. Square Planar vs Tetrahedral Coordination in Diamagnetic Complexes of Nickel(II) Containing Two Bidentate π -Radical Monoanions. *Inorg. Chem.* **2005**, *44*, 3636–3656.
- (32) Pfirmann, S.; Limberg, C.; Herwig, C.; Knispel, C.; Braun, B.; Bill, E.; Stösser, R. A Reduced β -Diketiminato-Ligated Ni₃H₄ Unit Catalyzing H/D Exchange. *J. Am. Chem. Soc.* **2010**, *132*, 13684–13691.
- (33) Rettenmeier, C.; Wadepohl, H.; Gade, L. H. Stereoselective Hydrodehalogenation via a Radical-Based Mechanism Involving T-Shaped Chiral Nickel(I) Pincer Complexes. *Chem. - Eur. J.* **2014**, *20*, 9657–9665.
- (34) Naveed, K.-u.-R.; Wang, L.; Yu, H.; Ullah, R. S.; Haroon, M.; Fahad, S.; Li, J.; Elshaarani, T.; Khan, R. U.; Nazir, A. Recent progress in the electron paramagnetic resonance study of polymers. *Polym. Chem.* **2018**, *9*, 3306–3335.
- (35) Stoll, S. *Encyclopedia of Biophysics*; Springer: Berlin, 2013.
- (36) Williams, V. A.; Hulley, E. B.; Wolczanski, P. T.; Lancaster, K. M.; Lobkovsky, E. B. Exploring the limits of redox non-innocence: pseudo square planar [$\{\kappa^4\text{-Me}_2\text{C}(\text{CH}_2\text{N}=\text{CHpy})_2\}\text{Ni}\}^n$ ($n = 2+, 1+, 0, -1, -2$) favor Ni(II). *Chem. Sci.* **2013**, *4*, 3636–3648.
- (37) Zimmermann, P.; Limberg, C. Activation of Small Molecules at Nickel(I) Moieties. *J. Am. Chem. Soc.* **2017**, *139*, 4233–4242.
- (38) Stanciu, C.; Jones, M. E.; Fanwick, P. E.; Abu-Omar, M. M. Multi-electron Activation of Dioxygen on Zirconium(IV) to Give an Unprecedented Bisperoxo Complex. *J. Am. Chem. Soc.* **2007**, *129*, 12400–12401.
- (39) Fukuzumi, S.; Ohkubo, K. Quantitative Evaluation of Lewis Acidity of Metal Ions Derived from the *g* Values of ESR Spectra of Superoxide: Metal Ion Complexes in Relation to the Promoting Effects in Electron Transfer Reactions. *Chem. - Eur. J.* **2000**, *6*, 4532–4535.
- (40) Petr, A.; Kataev, V.; Büchner, B. First Direct In Situ EPR Spectroelectrochemical Evidence of the Superoxide Anion Radical. *J. Phys. Chem. B* **2011**, *115*, 12036–12039.
- (41) Teles, J. H.; Hermans, I.; Franz, G.; Sheldon, R. A. Oxidation. *Ullmann's Encyclopedia of Industrial Chemistry*; Wiley-VCH, 2015.
- (42) Sahu, S.; Goldberg, D. P. Activation of Dioxygen by Iron and Manganese Complexes: A Heme and Nonheme Perspective. *J. Am. Chem. Soc.* **2016**, *138*, 11410–11428.
- (43) Wei, Y.; Li, H.; Yue, F.; Xu, Q.; Wang, J.; Zhang, Y. Oxidation mechanism of molecular oxygen over cyclohexene catalyzed by a cobalt *L*-glutamic acid complex. *RSC Adv.* **2016**, *6*, 107104–107108.
- (44) Kohantorabi, M.; Gholami, M. R. Cyclohexene oxidation catalyzed by flower-like core-shell Fe₃O₄@Au/metal organic frameworks nanocomposite. *Mater. Chem. Phys.* **2018**, *213*, 472–481.
- (45) Wind, M.-L.; Hoof, S.; Braun-Cula, B.; Herwig, C.; Limberg, C. Routes to Heterotrinary Metal Siloxide Complexes for Cooperative Activation of O₂. *Inorg. Chem.* **2020**, *59*, 6866–6875.
- (46) Wind, M.-L.; Braun-Cula, B.; Schax, F.; Herwig, C.; Limberg, C. A Polysiloxide Complex with two Chromium(III) η_2 -Superoxo Moieties. *Isr. J. Chem.* **2020**, *60*, 1057–1060.
- (47) Pirovano, P.; Farquhar, E. R.; Swart, M.; Fitzpatrick, A. J.; Morgan, G. G.; McDonald, A. R. Characterization and Reactivity of a Terminal Nickel(III)–Oxygen Adduct. *Chem. - Eur. J.* **2015**, *21*, 3785–3790.
- (48) Sheldrick, G. M. SADABS; University of Göttingen: Göttingen, Germany, 1996.
- (49) Sheldrick, G. M. SHELXT—Integrated space-group and crystal-structure determination. *Acta Crystallogr., Sect. A: Found. Adv.* **2015**, *71*, 3–8.
- (50) Sheldrick, G. M. Crystal structure refinement with SHELXL. *Acta Crystallogr., Sect. A: Found. Adv.* **2015**, *71*, 3–8.
- (51) Viculis, L. M.; Mack, J. J.; Mayer, O. M.; Hahn, H. T.; Kaner, R. B. Intercalation and exfoliation routes to graphite nanoplatelets. *J. Mater. Chem.* **2005**, *15*, 974–978.
- (52) Huang, Z.; Song, K.; Liu, F.; Long, J.; Hu, H.; Gao, H.; Wu, Q. Synthesis and characterization of a series of 2-aminopyridine nickel(II) complexes and their catalytic properties toward ethylene polymerization. *J. Polym. Sci., Part A: Polym. Chem.* **2008**, *46*, 1618–1628.
- (53) Wind, M.-L.; Hoof, S.; Herwig, C.; Braun-Cula, B.; Limberg, C. The Influence of Alkali Metal Ions on the Stability and Reactivity of Chromium(III) Superoxide Moieties Spanned by Siloxide Ligands. *Chem. - Eur. J.* **2019**, *25*, 5743–5750.
- (54) Mader, E. A.; Larsen, A. S.; Mayer, J. M. Hydrogen Atom Transfer from Iron(II)–Tris[2,2'-bi(tetrahydropyrimidine)] to TEMPO: A Negative Enthalpy of Activation Predicted by the Marcus Equation. *J. Am. Chem. Soc.* **2004**, *126*, 8066–8067.